Theoretical Estimation of the Acoustic Energy Generation and Absorption Caused by Jet Oscillation

Kin'ya Takahashi[1], Sho Iwagami[1], Taizo Kobayashi[2,3], and Toshiya Takami[3]

[1]*The Physics Laboratories, Kyushu Institute of Technology, Kawazu 680-4, Iizuka 820-8502, Japan*

[2]*Faculty of Fukuoka Medical Technology, Teikyo University, 6-22 Misaki-machi, Omuta 836-8505, Japan*

[3]*Research Institute for Information Technology, Kyushu University, 6-10-1 Hakozaki, Higashi-ku, Fukuoka 812-8581, Japan*

We investigate the energy transfer between the fluid field and acoustic field caused by a jet driven by an acoustic particle velocity field across it, which is the key to understanding the aerodynamic sound generation of flue instruments, such as the recorder, flute, and organ pipe. Howe's energy corollary allows us to estimate the energy transfer between these two fields. For simplicity, we consider the situation such that a free jet is driven by a uniform acoustic particle velocity field across it. We improve the semi-empirical model of the oscillating jet, i.e., exponentially growing jet model, which has been studied in the field of musical acoustics, and introduce a polynomially growing jet model so as to apply Howe's formula to it. It is found that the relative phase between the acoustic oscillation and jet oscillation, which changes with the distance from the flue exit, determines the quantity of the energy transfer between the two fields. The acoustic energy is mainly generated in the downstream area, but it is consumed in the upstream area near the flue exit in driving the jet. This theoretical examination well explains the numerical calculation of Howe's formula for the two-dimensional flue instrument model in our previous work [Fluid Dyn. Res. **46**, 061411 (2014)] as well as the experimental result of Yoshikawa *et al.* [J. Sound Vib. **331**, 2558 (2012)].

1. Introduction

Understanding the sound generation of edge tone and flue instruments, such as the recorder, flute, and organ pipe, is a long-standing problem in the fields of fluid dynamics, aero-acoustics, and musical acoustics, and it is still not understood completely.[1–3)] The sound source of these systems is an oscillating jet colliding with an edge, which is regarded as an

aerodynamic sound source. The generation mechanism of the aerodynamic sound, which is caused by the unsteady motion of a fluid flow with non-zero vorticities, has attracted many authors' attention since Lighthill introduced an acoustically analogous interpretation of aerodynamic sound generation, the so-called Lighthill's acoustic analogy.[3,4] However, the handling of Lighthill's inhomogeneous wave equation is not easy because its quadrupole source generates not only acoustic oscillations propagating to a far field but also a pseudo-sound pressure (or fluid pressure) in a near field.[5–7] Vortex sound theory, which was introduced by Powell and rigorously formulated by Howe, gives a physically interesting interpretation of the aerodynamic sound generation that the unsteady motion of vortices is the main source of aerodynamic sound.[3,8,9] However, in Howe's formula, acoustic oscillations are regarded as oscillations of stagnant enthalpy instead of those of pressure or air density so that one runs into trouble when attempting to apply.

An alternative method was proposed by Howe, i.e., Howe's energy corollary, which allows us to estimate the energy transfer between a fluid field and an acoustic field not in a direct way but in an indirect way.[3,10] Actually, Howe introduced an integral formula, which estimates the increase or decrease in the kinetic energy of the fluid field (solenoidal velocity field) due to the interaction with the acoustic field. In other words, the decrease and increase in the kinetic energy of the fluid field indicate the generation and absorption of the acoustic energy, respectively. However, there is a drawback to Howe's formula in real applications. It requires knowledge of the acoustic field, which is assumed to be completely separate from the fluid field. It is almost impossible to completely separate the acoustic field from the data of a compressible fluid field obtained by experiments and numerical simulations. Nevertheless, some approximate methods to calculate Howe's formula have recently been developed on the basis of experiments on flue instruments and cavity noise by several authors.[11–13] The idea of these methods is applicable to the numerical study of aerodynamic sound generation.[14]

In recent studies, we have developed a numerical technique to calculate the acoustic oscillations and fluid motion of two-dimensional (2D) and three-dimensional (3D) flue instrument models by performing a compressible large-eddy simulation (LES) and have succeeded in reproducing the basic properties of flue instruments, such as the relation between jet velocity and sound frequency.[15] Furthermore, we have improved the method introduced by the experimentalists to calculate Howe's formula numerically.[14] As a result, we have found that the oscillation of the jet generates most of the acoustic energy and that the vortices shed by its collision with the edge contribute to the absorption of acoustic energy rather than its generation [the configuration of the mouth opening shown in Fig. 1(a)]. This finding agrees with

Howe's theoretical prediction, which was made by combining many theoretical tools.[3] Furthermore, the acoustic energy is mainly created in the downstream area of the jet close to the edge and it seems to be consumed in the upstream area near the flue exit in synchronizing the jet motion with the acoustic oscillation excited in the resonance pipe. This was also confirmed in the experimental estimation of Howe's formula by Yoshikawa *et al.*[13]

In this paper, we focus on the energy transfer between the fluid field and the acoustic field caused by a jet driven by an acoustic particle velocity field $\boldsymbol{u}$, i.e., the velocity of the medium across the mouth opening in acoustic oscillation [see Fig.1 (a)]. This is the key to understanding the sound generation of flue instruments. We gave a brief theoretical explanation of the results obtained experimentally and numerically in the previous studies.[13,14] To analyze in detail the energy transfer between the solenoidal velocity field $\boldsymbol{v}$ and acoustic particle velocity field $\boldsymbol{u}$ in the area of the mouth opening using Howe's formula, we consider the simplified situation shown in Fig. 1 (b). Namely, a free jet is driven by a uniform acoustic particle velocity field across it. The dynamics of a jet driven by an acoustic field has been studied by many authors in the field of musical acoustics and a reliable semi-empirical model has been proposed.[1,16–21] However, the jet motion in the free jet model is considerably different from that of a flue instrument due to the nonexistence of the edge and resonance pipe.[15] Thus, we need to improve the free jet model so as to adjust it to the jet motion of a flue instrument. Then we can apply Howe's formula to it and investigate the energy transfer between the fluid field and acoustic field along the oscillating jet in comparison with the numerical results in the previous study.[14]

The organization of this paper is as follows. In Sect. 2, we briefly review Howe's energy corollary.[3,10] We introduce Howe's integral Π_g, which estimates the acoustic energy generated in a domain of integration and whose integrand Π_{gker} gives a spatial distribution that describes the local energy transfer between the fluid field and acoustic field.

In Sect. 3, we introduce the semi-empirical model of the jet motion disturbed by the uniform acoustic field across it, which has been studied in the field of musical acoustics.[1,16–21] We propose some improvements to the model to adjust the jet motion in the free jet model to that in the flue instrument model and to apply Howe's energy corollary to it. First, we introduce polynomially growing amplitude models instead of exponentially growing amplitude models (exponential-type and cosh-type), which have been traditionally studied. This is because the amplitude growth of the hydrodynamic wave formed by the jet diverges from the exponential function at some distance from the flue exit. Since the semi-empirical model describes only the behavior of the centerline of the jet, we next propose a method to approxi-

(a)

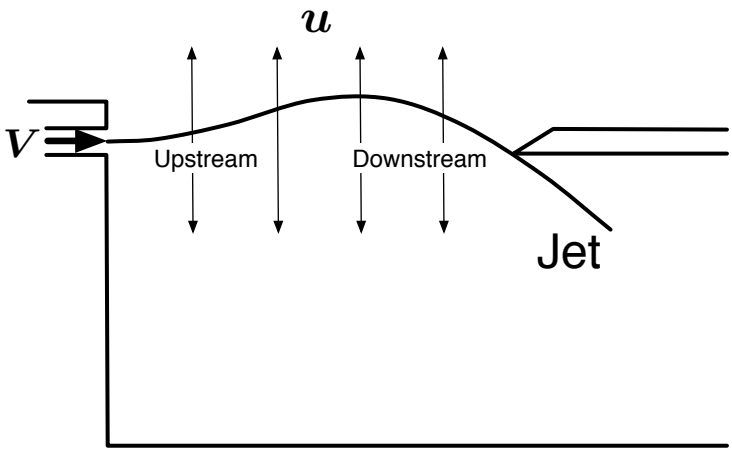

(b)

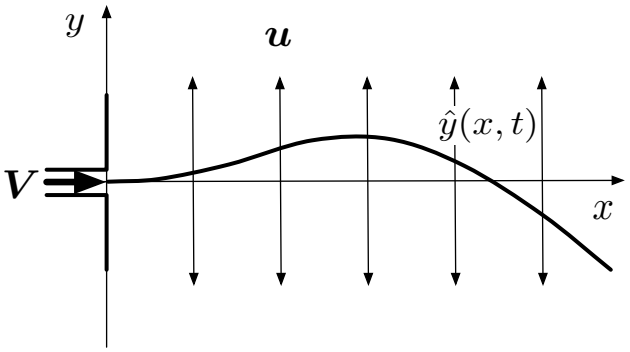

Fig. 1. Schematic drawing of the jet of a flue instrument and the jet model with vertical acoustic particle velocity $\boldsymbol{u}$. (a) Operating portion of a flue instrument. (b) Profile of the jet model $\hat{y}(x,t)$.

mately reproduce the velocity distribution along a wavy jet, whose streamwise velocity profile at a particular cross section is approximated by a sech^2-type function.[1,16] Finally, Howe's energy corollary is applied to the wavy jet models, and mathematical expressions for Π_g and Π_{gker} are obtained. The distribution of Π_{gker} is qualitatively the same as those obtained numerically and experimentally in the previous works.[13,14] The mathematical formulae for Π_g and Π_{gker} indicate that the relative phase between the acoustic oscillation and jet oscillation, which changes with the distance from the flue exit, is the key to understanding the energy transfer between the acoustic field and the fluid field. Actually, a small amount of acoustic energy absorption occurs in the upstream area, but the acoustic energy is mainly generated in the downstream area.

In Sect. 4, to confirm the validity of the theoretical estimation in Sect. 3, we compare the values of Π_{gker} and Π_g obtained by the jet models with the numerical results of the 2D flue instrument model, which was investigated in our previous study.[14] First we review the numerical simulation of the 2D flue instrument model. We introduce the 2D flue instrument model and show the results for Π_{gker} and Π_g and the time average of Π_g, i.e., E_a, calculated for this model. We take small domains of integration rather than large domains in order to obtain detailed information on the acoustic energy generation and absorption along the jet. That is, the area between the flue exit and the edge is divided into five domains, while it was divided into two domains in the previous study.[14] Next, to clarify which of the jet models, exponential or polynomial models, shows better agreement with the numerical results for the 2D flue instrument model, we compare the jet profiles of the exponential and polynomial models with that of the 2D flue instrument model. We also calculate the time average E_a for each model compared with that for the 2D flue instrument model. The time average E_a for the cubic model takes a value close to that for the 2D flue instrument model in every domain of integration. This shows that the cubic polynomial model most closely reproduces the properties of the jet motion in the 2D flue instrument model. Finally, by using the cubic model, we quantitatively investigate the properties of Π_{gker} as well as those of Π_g region by region in comparison with the numerical results for the 2D flue instrument model. The integrand Π_{gker} is very similar in distribution to that for the 2D flue instrument model. The integral Π_g in each domain of integration shows the same tendencies in amplitude and phase as those for the 2D flue instrument model. Therefore, the jet model introduced in this paper well explains the energy transfer along the oscillating jet between the fluid field and acoustic field with the help of Howe's energy corollary. We conclude that the acoustic energy is mainly generated in the downstream area near the edge. Sect. 5 is devoted to a summary and discussion.

2. Howe's Energy Corollary

Howe introduced a method to estimate, not in a direct way but in an indirect way, the generation and absorption of acoustic energy through the interaction with an unsteady fluid flow.[3,10] The change in the kinetic energy of a high-Reynolds-number isentropic flow in a volume V is given by the following integral formula:

$$\Pi = \frac{1}{2}\rho_0 \frac{\partial}{\partial t} \iiint_V \boldsymbol{v}^2 \, dV \approx \rho_0 \iiint_V (\boldsymbol{\omega} \times \boldsymbol{v}) \cdot \boldsymbol{u} \, dV, \tag{1}$$

where $\boldsymbol{v}$, $\boldsymbol{\omega}$, and $\boldsymbol{u}$ denote the fluid velocity (solenoidal velocity), vorticity, and acoustic particle velocity, respectively, and ρ_0 is the air density of the equilibrium atmosphere. The integral

Π indicates the change in the kinetic energy of the fluid flow in the volume V induced by the interaction with an acoustic field. Conversely, it means that the net sound absorption (or generation) in the volume V is due to the interaction with the fluid field if it takes a positive (or negative) value.

Furthermore, one can assume that the integrand $\Pi_{ker} = \rho_0(\boldsymbol{\omega}\times\boldsymbol{v})\cdot\boldsymbol{u}$ indicates the local energy transfer between the fluid field and acoustic field. Namely, it takes a negative (or positive) value when the generation (or absorption) of acoustic energy occurs. For later convenience, we introduce the integral and integrand with opposite signs, $\Pi_g = -\Pi$ and $\Pi_{gker} = -\Pi_{ker}$.[14)]

In order to calculate Howe's integral, one needs the acoustic particle velocity $\boldsymbol{u}$ separate from the total fluid particle velocity of the compressible fluid $\bar{\boldsymbol{v}}$, which is decomposed as $\bar{\boldsymbol{v}} = \boldsymbol{v}+\boldsymbol{u}+\boldsymbol{u}_n$, where $\boldsymbol{u}_n$ is the nonlinear compressible component of $\bar{\boldsymbol{v}}$ and is usually negligible.[14)] Normally, $\boldsymbol{u}$ is much smaller than $\bar{\boldsymbol{v}}$ ($\approx \boldsymbol{v}$), and it is not easy to calculate $\boldsymbol{u}$ with accuracy from the data of $\bar{\boldsymbol{v}}$ obtained experimentally or numerically. For the case of flue instruments, such as the recorder and organ pipe, $\boldsymbol{u}$ is rather large and is not negligibly small compared with $\bar{\boldsymbol{v}}$ because it is enhanced by the pipe resonance. Nevertheless, in order to obtain $\boldsymbol{u}$, an approximate method making use of the resonance pipe has recently been developed on the basis of experiments.[11,13)] Namely, it is assumed that the acoustic resonance field generated by a sound generator (loudspeaker) attached at the remote end of a pipe well approximates the acoustic field near the mouth opening of an instrument driven by a jet. Howe's integrand and integral obtained by combining the acoustic particle velocity generated by the sound generator with the fluid data observed for the jet-driven pipe seem to provide physically reasonable values.

In a recent study,[14)] we introduced a method, which is a numerical analog to the approximate method based on experiments, and applied it to the calculation of a small organ pipe model, which gives essentially the same results as those obtained experimentally. In this paper, we concentrate on giving a theoretical explanation for the generation mechanism of acoustic energy from an oscillating jet. To do this, we introduce a simple model of an oscillating jet driven by an acoustic field across it.

3. Models of the Oscillating Jet

3.1 Semi-empirical model and velocities on the centerline of a wavy jet

It is considered in the cases of edge tone and flue instruments that the jet oscillation is induced by the alternating fluid velocity (or acoustic particle velocity) in the vertical direction.[1,3)] Note that the local particle velocity of the acoustic field near the jet can be approx-

imately regarded as the alternating velocity of the incompressible fluid if its wavelength is sufficiently large compared with the jet thickness. For the sake of simplicity, we omit the edge and consider a jet driven by an acoustic particle velocity field in the vertical direction. According to the textbook written by Fletcher and Rossing[1] and recent studies,[17–21] when the jet is driven by a uniform acoustic field with the velocity

$$u_y = u_0 \cos \omega t, \tag{2}$$

the displacement in the y-direction of the centerline of the jet is given by

$$\hat{y}(x,t) = \frac{u_0}{\omega}\Big(\sin \omega t - g(\mu x) \sin \omega(t - x/u_w)\Big), \tag{3}$$

where the flue exit exists at the origin and its centerline is placed along the x-axis so that the acoustic field exists in the semi-infinite space $x > 0$ [see Fig. 1(b)]. This means that the jet forms a hydrodynamic wave with phase speed u_w and its amplitude is determined as an increasing function $g(\mu x)$ with rate μ. If the jet velocity at the flue exit V is given, the phase speed u_w is approximately obtained as $u_w \approx V/2$.[1,15] When the jet is not extremely narrow, the approximation $\mu \approx k = \omega/u_w$ is also used.[1,15]

Fletcher and coworkers took $g(\mu x)$ as[1,17]

$$g(\mu x) = \cosh \mu x, \tag{4}$$

but the several authors have pointed out that the exponential model

$$g(\mu x) = \exp \mu x \tag{5}$$

is better fitted to observations.[18–21] Actually, the exponential model well approximates the wave profile near the flue exit. However, at some distance from the flue exit, the growth of the wave amplitude diverges from the exponential function. Thus, we introduce a polynomial approximation with degree n:

$$g(\mu x) = \sum_{k=0}^{n} \frac{1}{k!}(\mu x)^k. \tag{6}$$

The fluid particle velocity $\boldsymbol{v}_L$ at the centerline of the jet can be obtained as the solution of the constrained motion of the particle as it propagates along a moving path $y = \hat{y}(x,t)$. First, when $|g(\mu x)| \ll 1$, we can simply assume that the x-component of $\boldsymbol{v}_L$ is constant and given as

$$v_{xL} = V. \tag{7}$$

Actually, it is expected that the jet velocity will not be significantly reduced between the flue exit and the edge (see Appendix). Thus, the x-component of the position of the fluid particle

is given by

$$x_L = Vt + x_0, \tag{8}$$

where x_0 is a constant. Substituting $x = x_L$ into $\hat{y}(x, t)$ in Eq. (3) and taking its total differential, we obtain the y-component of the fluid particle velocity on the centerline:

$$\begin{aligned} v_{yL}(x_L, t) = \frac{\mathrm{d}}{\mathrm{d}t}\hat{y}(x_L, t) &= \frac{\partial}{\partial t}\hat{y}(x_L, t) + v_{xL}\frac{\partial}{\partial x_L}\hat{y}(x_L, t) \\ &= u_0\Big(\cos\omega t + (v_{xL}/u_w - 1)g(\mu x_L)\cos\omega(t - x_L/u_w) \\ &\quad -\frac{\mu v_{xL}}{\omega}g'(\mu x_L)\sin\omega(t - x_L/u_w)\Big), \end{aligned} \tag{9}$$

where $g'(x)$ denotes the derivative of $g(x)$. At $x_L = 0$, Eq. (9) gives the y-component of the fluid velocity at the flue exit,

$$\begin{aligned} v_{yL}(x_L = 0, t) &= u_0 v_{xL}\Big[\frac{1}{u_w}g(0)\cos\omega t - \frac{\mu}{\omega}g'(0)\sin\omega t\Big] \\ &\approx 2u_0(g(0)\cos\omega t - g'(0)\sin\omega t). \end{aligned} \tag{10}$$

Here, we make use of Eq. (7) together with the approximations $u_w \approx V/2$ and $\mu \approx k = \omega/u_w$. For the cosh model (4) with $g(0) = 1$ and $g'(0) = 0$, the fluid velocity v_{yL} is synchronized with the acoustic particle velocity u_y at the flue exit and its amplitude is almost twice as large as that of u_y. On the other hand, for the exponential function model (5) and polynomial model (6) with $g(0) = 1$, $g'(0) = 1$, the amplitudes of v_{yL} are $2\sqrt{2}$ times larger than that of u_y at the flue exit, and v_{yL} leads u_y in phase by $\pi/4$ because $\cos\omega t - \sin\omega t = \sqrt{2}\cos(\omega t + \pi/4)$ in Eq. (10). It is numerically confirmed that the values of v_{yL} for the exponential and polynomial models are synchronized with that of u_y at small distances from the flue exit.

3.2 Reproduction of velocity distribution along a wavy jet

In this subsection, we explain how to reproduce the velocity distribution along a wavy jet. First, we consider the case of an inviscid flow without the disturbance of an acoustic field. Thus, the jet propagates in a straight line with a constant thickness. Then, the y-component of the velocity is zero, $v_y = 0$, and the x-component v_x is independent of x and time, namely v_x is a function of y, i.e., $v_x(y)$. It is reasonable that the distribution of v_x has a bell-shaped profile, which is well approximated by a sech^2-type function.[1,16–21] Thus, the velocity $\boldsymbol{v}$ is represented as

$$v_x = V\mathrm{sech}^2(y/b) \equiv f(y/b), \quad v_y = 0, \tag{11}$$

where b is a parameter that determines the semithickness of the jet and the function $f(y/b)$ is introduced for convenience in the following calculations.

Let us obtain the velocity distribution along a wavy jet that satisfies the incompressible fluid condition div $\boldsymbol{v} = 0$. The velocity $\boldsymbol{v}$ should take values given by eqs.(7) and (9) at the centerline of the jet. We set the profile of v_x at a fixed value of x to be the same as the first equation of Eq. (11) with its center at $\hat{y}(x,t)$ given by Eq. (3). In order to satisfy the incompressible fluid condition div $\boldsymbol{v} = 0$, v_x and v_y should be represented as

$$v_x = V\mathrm{sech}^2((y-\hat{y}(x,t))/b), \tag{12}$$

$$v_y = \frac{\partial}{\partial t}\hat{y}(x,t) + v_x\frac{\partial}{\partial x}\hat{y}(x,t). \tag{13}$$

Concretely, Eq. (13) is written as

$$\begin{aligned} v_y = {} & u_0\Big\{\cos\omega t + \Big[\frac{V}{u_w}\mathrm{sech}^2((y-\hat{y}(x,t))/b) - 1\Big]g(\mu x)\cos\omega(t-x/u_w) \\ & -\frac{\mu}{\omega}V\mathrm{sech}^2((y-\hat{y}(x,t))/b)g'(\mu x)\sin\omega(t-x/u_w)\Big\}, \end{aligned} \tag{14}$$

which coincides with Eq. (9) at $y = \hat{y}(x,t)$.

3.3 Howe's energy corollary applied for wavy jet models

Since the acoustic particle velocity $\boldsymbol{u}$ only has a y-component, which is alternately directed upward and downward, Π_{gker} is represented as

$$\Pi_{gker} = \rho_0(\boldsymbol{v}\times\boldsymbol{\omega})\cdot\boldsymbol{u} = -\rho_0\omega_z v_x u_y = \rho_0\Big(\frac{\partial v_x}{\partial y} - \frac{\partial v_y}{\partial x}\Big)v_x u_y. \tag{15}$$

Substituting the components of the jet velocity given by Eqs. (12) and (13), Eq. (15) is written as

$$\begin{aligned} \Pi_{gker} = {} & \Big(\frac{1}{b}f'((y-\hat{y}(x,t))/b) - \frac{\partial^2\hat{y}}{\partial t\partial x} - v_x\frac{\partial^2\hat{y}}{\partial x^2} - \frac{\partial v_x}{\partial x}\frac{\partial\hat{y}}{\partial x}\Big)\rho_0 v_x u_y \\ = {} & \Big\{\Big[\frac{1}{b}f'((y-\hat{y}(x,t))/b)\Big(1+\Big(\frac{\partial\hat{y}}{\partial x}\Big)^2\Big)\Big] - \Big[\frac{\partial^2\hat{y}}{\partial t\partial x} + v_x\frac{\partial^2\hat{y}}{\partial x^2}\Big]\Big\}\rho_0 v_x u_y, \end{aligned} \tag{16}$$

where the orders of the first and second terms in the final line are respectively estimated as

$$\Big[\frac{1}{b}f'((y-\hat{y}(x,t))/b)\Big(1+\Big(\frac{\partial\hat{y}}{\partial x}\Big)^2\Big)\Big]\rho_0 v_x u_y \approx O(V^2u_0/b) + O(u_0^3/b\times g(\mu x)^2) \tag{17}$$

and

$$-\Big[\frac{\partial^2\hat{y}}{\partial t\partial x} + v_x\frac{\partial^2\hat{y}}{\partial x^2}\Big]\rho_0 v_x u_y \approx O(u_0^2\omega\times g(\mu x)). \tag{18}$$

For comparison with the previous work, in which Howe's formula is numerically estimated for the 2D flue instrument model,[14] the parameters are set as $u_0 = 0.5$ m/s, $V = 12$ m/s, $b = 0.5\times10^{-3}$ m, and $\omega = 2\pi f$ with $f = 830$ Hz. Then, the first term, estimated as $O(10^5)$,

is much larger than the second term of $O(10^3 \times g(\mu x))$, and Π_{gker} is seemingly governed by the first term. Since the function $f(y)$ defined by Eq. (11) is an even function, the first term becomes an odd function of $y - \hat{y}(x,t)$. Thus, the integral of the first term with respect to y from $-\infty$ to ∞ is zero and does not contribute to the integral Π_g. On the other hand, the second term is an even function of $y - \hat{y}(x,t)$ and makes a contribution to Π_g. Thus, the creation and absorption of acoustic energy should be caused by the second term. Namely, the even-function parts of $\frac{\partial v_y}{\partial x}$, i.e., $\frac{\partial^2 \hat{y}}{\partial t \partial x} + v_x \frac{\partial^2 \hat{y}}{\partial x^2}$, change with x and control the quantity of the contributions.

Let us examine this in more detail. The first term in the final line of Eq. (16), i.e., Eq. (17), is written as

$$\begin{aligned}
&\left[\frac{1}{b} f'((y-\hat{y}(x,t))/b)\left(1+\left(\frac{\partial \hat{y}}{\partial x}\right)^2\right)\right]\rho_0 v_x u_y \\
&\quad = \frac{\rho_0}{b} f'((y-\hat{y}(x,t))/b) f((y-\hat{y}(x,t))/b)\left(1+\left(\frac{\partial \hat{y}}{\partial x}\right)^2\right)u_y \\
&\quad = -\frac{2\rho_0 u_y V^2}{b}\frac{\sinh(y-\hat{y}(x,t))}{\cosh^5(y-\hat{y}(x,t))} \\
&\quad \left[1+\left(\frac{u_0}{u_w} g(\mu x)\ \cos\omega(t-x/u_w) - \frac{\mu u_0}{\omega} g'(\mu x)\ \sin\omega(t-x/u_w)\right)^2\right]. \qquad (19)
\end{aligned}$$

Using the approximation $\mu \approx k = \omega/u_w$, it is further reduced to

$$\begin{aligned}
&\left[\frac{1}{b} f'((y-\hat{y}(x,t))/b)\left(1+\left(\frac{\partial \hat{y}}{\partial x}\right)^2\right)\right]\rho_0 v_x u_y \\
&\approx -\frac{2\rho_0 u_y V^2}{b}\frac{\sinh(y-\hat{y}(x,t))}{\cosh^5(y-\hat{y}(x,t))}\left[1+\frac{u_0^2}{u_w^2}(g(\mu x)\cos\omega(t-x/u_w) - g'(\mu x)\sin\omega(t-x/u_w))^2\right] \\
&= -\frac{2\rho_0 u_0 V^2}{b}\frac{\sinh(y-\hat{y}(x,t))}{\cosh^5(y-\hat{y}(x,t))}\Big[\cos\omega t + \frac{u_0^2}{u_w^2}\Big(\frac{1}{2}(g(\mu x)^2 + g'(\mu x)^2)\cos\omega t \\
&\qquad + \frac{1}{4}(g(\mu x)^2 - g'(\mu x)^2)(\cos(\omega t - 2\omega x/u_w) + \cos(3\omega t - 2\omega x/u_w)) \\
&\qquad - \frac{1}{2} g(\mu x) g'(\mu x)\ (\sin(\omega t - 2\omega x/u_w) + \sin(3\omega t - 2\omega x/u_w))\Big)\Big], \qquad (20)
\end{aligned}$$

where Eq. (2) is made use of in the right-hand side. Equation (20) indicates that the time average of the first term, i.e., Eq. (17), is zero. Since the sum of the terms in the square brackets [...] in the middle of Eq. (20) takes a positive value, then if $u_y > 0$, the first term takes negative and positive values along the upper and lower sides of the jet, respectively, and if $u_y < 0$, it takes opposite values, i.e., positive along the upper side and negative along the lower side.

The second term in the final line of Eq. (16), i.e., Eq. (18), is rewritten as

$$-\Big[\frac{\partial^2\hat{y}}{\partial t\partial x}+v_x\frac{\partial^2\hat{y}}{\partial x^2}\Big]\rho_0 v_x u_y = \rho_0 u_0 v_x u_y\Big[\mu\Big(1-\frac{2v_x}{u_w}\Big)g'(\mu x)\ \cos\omega(t-x/u_w) + \Big(\frac{\omega}{u_w}\Big(1-\frac{v_x}{u_w}\Big)g(\mu x)+\frac{\mu^2 v_x}{\omega}g''(\mu x)\Big)\sin\omega(t-x/u_w)\Big)\Big]. \quad (21)$$

Using the approximation $\mu \approx k = \omega/u_w$, it is reduced to

$$\begin{aligned}-\Big[\frac{\partial^2\hat{y}}{\partial t\partial x}+v_x\frac{\partial^2\hat{y}}{\partial x^2}\Big]\rho_0 v_x u_y &\approx \frac{\rho_0 u_0 v_x u_y\omega}{u_w}\Big[\Big(1-\frac{2v_x}{u_w}\Big)g'(\mu x)\ \cos\omega(t-x/u_w) \\ &\quad +\Big(g(\mu x)+\frac{v_x}{u_w}(g''(\mu x)-g(\mu x))\Big)\sin\omega(t-x/u_w)\Big] \\ &= \frac{\rho_0 u_0^2 v_x\omega}{2u_w}\Big[\Big(1-\frac{2v_x}{u_w}\Big)g'(\mu x)\ (\cos(2\omega t-\omega x/u_w)+\cos\omega x/u_w) \\ &\quad +\Big(g(\mu x)+\frac{v_x}{u_w}(g''(\mu x)-g(\mu x))\Big)\ (\sin(2\omega t-\omega x/u_w)-\sin\omega x/u_w)\Big],\end{aligned} \quad (22)$$

where we made use of Eq. (2) in the right-hand side. The time average of Π_{gker} is obtained as

$$\bar{\Pi}_{gker}=\frac{\rho_0 u_0^2 v_x\omega}{2u_w}\Big[\Big(1-\frac{2v_x}{u_w}\Big)g'(\mu x)\cos\omega x/u_w-\Big(g(\mu x)+\frac{v_x}{u_w}(g''(\mu x)-g(\mu x))\Big)\sin\omega x/u_w\Big], \quad (23)$$

so that the second term, i.e., Eq. (18), contributes to the net generation and absorption of acoustic energy. On the other hand, using Eq. (12) together with $(\tanh z)' = \mathrm{sech}^2 z$ and $(\tanh z)' - (\frac{1}{3}\tanh^3 z)' = \mathrm{sech}^4 z$, the integral of Π_{gker} with respect to y is represented as

$$\begin{aligned}\Pi_{gy} \equiv \int_{-\infty}^{\infty}\Pi_{gker}\,\mathrm{d}y &= \frac{\rho_0 u_0^2 Vb\omega}{u_w}\Big[\Big(1-\frac{4V}{3u_w}\Big)g'(\mu x)(\cos(2\omega t-\omega x/u_w)+\cos\omega x/u_w) \\ &\quad +\Big(g(\mu x)+\frac{2V}{3u_w}(g''(\mu x)-g(\mu x))\Big)(\sin(2\omega t-\omega x/u_w)-\sin\omega x/u_w)\Big].\end{aligned} \quad (24)$$

Furthermore, the integral of $\bar{\Pi}_{gker}$ with respect to y, i.e., the time average of the above integral, becomes

$$\begin{aligned}\bar{\Pi}_{gy} \equiv \int_{-\infty}^{\infty}\bar{\Pi}_{gker}\,\mathrm{d}y &= \frac{\rho_0 u_0^2 Vb\omega}{u_w}\Big[\Big(1-\frac{4V}{3u_w}\Big)g'(\mu x)\cos\omega x/u_w \\ &\quad -\Big(g(\mu x)+\frac{2V}{3u_w}(g''(\mu x)-g(\mu x))\Big)\sin\omega x/u_w\Big].\end{aligned} \quad (25)$$

Note that $1-\frac{4V}{3u_w} < -1$ in the first term of the right-hand side because $u_w \approx V/2$.

For the exponential model (5), $\bar{\Pi}_{gy}$ is given by

$$\bar{\Pi}_{gy}=\int_{-\infty}^{\infty}\bar{\Pi}_{gker}\,\mathrm{d}y=\frac{\rho_0 u_0^2 Vb\omega}{u_w}\Big[\Big(1-\frac{4V}{3u_w}\Big)\cos\omega x/u_w-\sin\omega x/u_w\Big]\exp\mu x. \quad (26)$$

In the case of $\mu x \approx \omega x/u_w \ll 1$, it is approximated as

$$\bar{\Pi}_{gy} = \int_{-\infty}^{\infty} \bar{\Pi}_{gker}\, \mathrm{d}y \approx \frac{\rho_0 u_0^2 V b \omega}{u_w}\Big[\Big(1 - \frac{4V}{3u_w}\Big) - \omega x/u_w\Big] \exp \mu x, \tag{27}$$

which takes a negative value. Since the absolute value of the coefficient of the cosine term is larger than that of the sine term in the right-hand side of Eq. (26) because $|1 - \frac{4V}{3u_w}| > 1$, the cosine function term dominates the sine function term except in the neighborhoods of $\omega x/u_w = (n + 1/2)\pi$. Therefore, in the range near $\pi/2 < \omega x/u_w < 3\pi/2$, where $\cos \omega x/u_w$ takes negative values, $\bar{\Pi}_{gy}$ becomes positive. More precisely, it is given by the following condition:

$$\Big(\frac{4V}{3u_w} - 1\Big) \cos \omega x/u_w + \sin \omega x/u_w < 0. \tag{28}$$

Introducing variables R and θ_c defined by $R \equiv \sqrt{(\frac{4V}{3u_w} - 1)^2 + 1}$ and $\theta_c \equiv \arctan(\frac{4V}{3u_w} - 1)$ $(0 < \theta_c < \pi/2)$, Eq. (28) is written as

$$R \sin(\omega x/u_w + \theta_c) < 0 \tag{29}$$

and the integral $\bar{\Pi}_{gy}$ takes positive values in the range $\pi - \theta_c < \omega x/u_w < 2\pi - \theta_c$.

For the polynomial model (6), $\bar{\Pi}_{gy}$ is represented as

$$\begin{aligned} \bar{\Pi}_{gy} = \int_{-\infty}^{\infty} \bar{\Pi}_{gker}\, \mathrm{d}y \quad = \quad & \frac{\rho_0 u_0^2 V b \omega}{u_w}\Big[\Big(1 - \frac{4V}{3u_w}\Big)\Big(\sum_{k=0}^{n-1} \frac{1}{k!}(\mu x)^k\Big) \cos \omega x/u_w \\ & -\Big(\Big(\sum_{k=0}^{n} \frac{1}{k!}(\mu x)^k\Big) - \frac{2V}{3u_w}\Big(\sum_{k=n-1}^{n} \frac{1}{k!}(\mu x)^k\Big)\Big) \sin \omega x/u_w\Big]. \end{aligned} \tag{30}$$

In the case of $\mu x \approx \omega x/u_w \ll 1$, it is estimated as

$$\bar{\Pi}_{gy} = \int_{-\infty}^{\infty} \bar{\Pi}_{gker}\, \mathrm{d}y \approx \frac{\rho_0 u_0^2 V b \omega}{u_w}\Big[\Big(1 - \frac{4V}{3u_w}\Big)(1 + \mu x) - \omega x/u_w\Big], \tag{31}$$

which takes negative values. According to a numerical estimation, the cosine function term dominates the sine function term when μx is not extremely large, and $\bar{\Pi}_{gy}$ becomes positive approximately in the range $\pi/2 < \omega x/u_w < 3\pi/2$. For the parameter values of the 2D flue instrument model, $f = 830$ Hz and $u_w = V/2 = 6$ m/s, it becomes positive in the range $1.8 < x < 5.4$mm for the cubic polynomial model. This means that acoustic energy generation occurs in the latter half of the jet close to the edge, which exists at $x = 5$mm for the 2D flue instrument model.[14,15] This finding agrees with the experimental and numerical results.[13,14]

4. Quantitative Estimation of Howe's Energy Corollary with the Wavy Jet Models

4.1 Review of numerical simulation of the 2D flue instrument model

In this section, we briefly explain the results of our recent work,[14] in which we applied Howe's energy corollary to a 2D flue instrument model and numerically estimated the acoustic energy generation and absorption induced by the interaction with the fluid flow, mainly with the oscillating jet.

The geometry of the 2D flue instrument model with a closed pipe is shown in Fig.2 and its dimensions are indicated in the figure caption. As shown in Sects. 2 and 3 in the previous paper,[14] the compressible large-eddy simulation (LES)[22] was used for a compressible fluid simulation of the 2D flue instrument model driven by jet injection from the flue channel. On the other hand, we used a second-order-in-time, fourth-order-in-space finite-difference time-domain method [FDTD(2,4)] to reproduce the resonance acoustic field in the pipe, which is excited by an acoustic pressure source attached on the far end wall of the pipe.

The calculation of Howe's integral was done as follows. First, by performing a compressible LES, the fluid and acoustic fields are simultaneously reproduced. The fluid velocity $\bar{\boldsymbol{v}}$ and vorticity $\boldsymbol{\omega}$ are observed near the mouth opening. The pressure fluctuation at point A on the far end (see Fig.2) is regarded as the acoustic pressure p, i.e., the fluctuation of the acoustic pressure from atmospheric pressure, because the fluid flow is negligibly small there.

Next, the resonance acoustic field is approximately reproduced by the FDTD. A sinusoidal pressure source is set on the far end wall to reproduce the acoustic pressure with the same frequency and almost the same amplitude as the pressure data obtained by the fluid simulation by the LES. Then, we obtain the acoustic particle velocity $\boldsymbol{u}$ near the mouth opening. In order to accurately adjust the phase of the acoustic field obtained by the FDTD to that obtained by the LES, we match the phase of the y-component of the acoustic particle velocity u_y with that of the y-component of the fluid velocity $\bar{v}_y$ at point B at a distance of 1 mm to the right of the flue exit and on the extension of the centerline of the flue as showing in Fig. 2. Then, we approximately obtain Howe's integrand Π_{gker}, i.e.,

$$\rho_0(\bar{\boldsymbol{v}} \times \boldsymbol{\omega}) \cdot \boldsymbol{u} = \rho_0((\boldsymbol{v} + \boldsymbol{u}_n) \times \boldsymbol{\omega}) \cdot \boldsymbol{u} \approx \rho_0(\boldsymbol{v} \times \boldsymbol{\omega}) \cdot \boldsymbol{u} = \Pi_{gker}, \tag{32}$$

and Howe's integral Π_g is estimated straightforwardly.

We briefly explain the numerical results: for details see the previous paper.[14] When the jet velocity V is taken as $V = 12$ m/s, the fluid simulation with the compressible LES generates a strong acoustic oscillation in the pipe, namely the maximum acoustic pressure p_0 above 100 Pa, and the fundamental frequency of the acoustic pressure p observed at point A is 830 Hz.

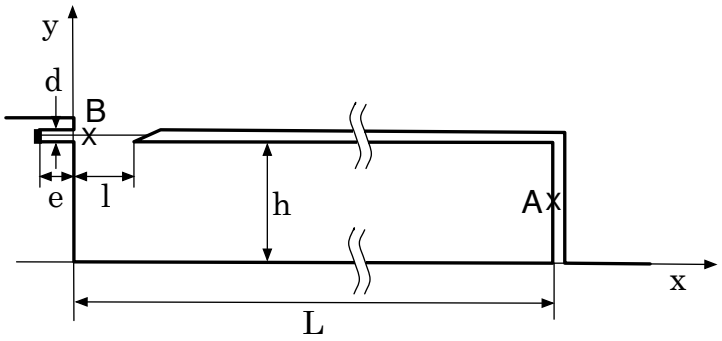

Fig. 2. 2D flue instrument model in the previous paper:[14] the height of the flue channel is $d = 1$ mm, the length of the flue channel is $e = 3$ mm, the width of the mouth aperture is $l = 5$ mm, the pipe length is $L = 90$mm, the pipe height is $h = 10$ mm, and the edge angle is taken as $\theta = 25°$.

Figures 3 (a) and (b) respectively show the spatial distribution of $|\bar{\boldsymbol{v}}|$ near the mouth opening and that of Π_{gker} together with the acoustic particle velocity $\boldsymbol{u}$ obtained by the FDTD, which is indicated by arrows. In this case, the acoustic particle velocity $\boldsymbol{u}$ is directed almost upward and Π_{gker} takes negative and positive values along the upper and lower sides of the jet, respectively, as theoretically predicted in Sect. 3.3. As also shown in this figure, the integral region of Π_{gker} is divided into several parts to find the area that contributes most to the acoustic energy generation and absorption. In particular, we focus on the acoustic energy generation and absorption caused by the jet motion. To do this, the area between the flue exit at $x = 0$mm and the top of the edge at $x = 5$mm is divided into five regions at even intervals from R1 to R5, although it was divided into two regions in the previous paper.[14] The regions under and over the edge, Ed and Eu, respectively, are the same as those in the previous paper.[14]

Integrating Π_{gker} over each region, we can obtain Π_g region by region. Figure 4 shows the time evolution of Π_g in regions R1 to R5 and the sum of these Π_g in the time interval $0.025 \leq t \leq 0.05$s, in which the stable oscillations of the jet and acoustic field are observed. For regions R1 and R2, Π_g takes small negative values for most of the time period. The fluctuation of Π_g in R2 slightly lags in phase behind that at R1. On the other hand, for regions R3, R4, and R5, Π_g takes positive values for large portions of the time period, in particular, it becomes positive almost all the time in R4. The amplitude of Π_g becomes larger with increasing region number. The fluctuation of Π_g in R5 slightly lags in phase behind that in R4. Furthermore, Π_g for R4 and R5 are almost out of phase by π compared with those for R1 and R2. However, the fluctuation of Π_g in R3 is rather irregular and it is difficult to compare it with the others. Since Π_g for R4 and R5 are much larger in amplitude than those for R1 and

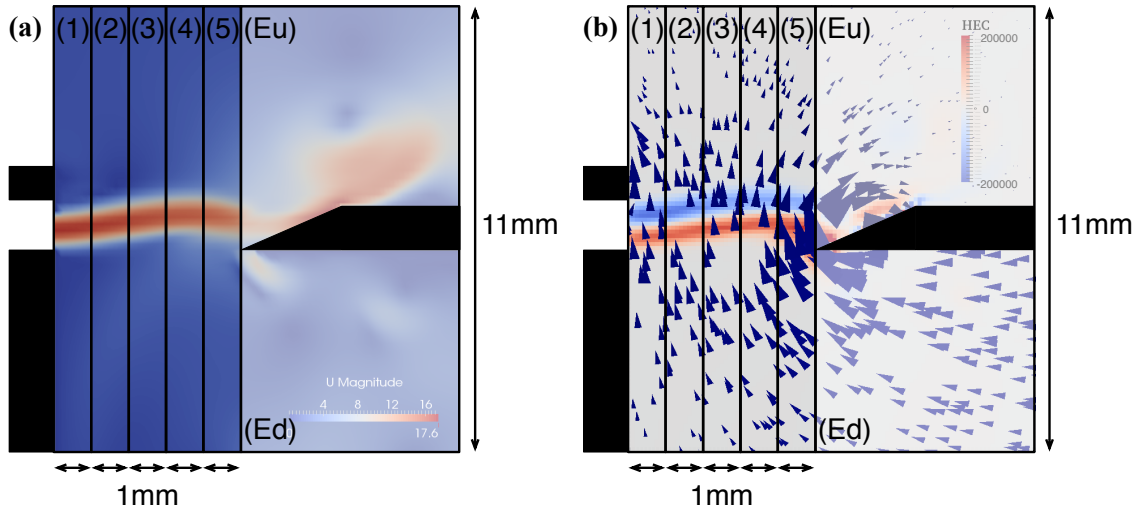

Fig. 3. (Color online) Numerical results obtained by the 2D flue instrument model. (a) Spatial distribution of $|\bar{\boldsymbol{v}}|$ near the mouth opening. (b) Spatial distribution of Π_{gker} and the acoustic particle velocity $\boldsymbol{u}$ indicated by arrows. The domains of integration of Π_{gker} are also shown; the labels (1),$\cdots$,(5), (Ed), and (Eu) indicate the regions R1,$\cdots$,R5, Ed, and Eu, respectively.

R2, the total Π_g, the sum of Π_g in regions R1 to R5, is almost in phase with those for R4 and R5 and takes positive values almost all the time.

To find the net energy transfer between the fluid field and the acoustic field, we calculate the time average of Π_g in each region, defined by

$$E_a = \frac{1}{t_2 - t_1} \int_{t_1}^{t_2} \Pi_g(t)\, \mathrm{d}t, \tag{33}$$

where the lower and upper limits of integration are taken at $t_1 = 0.025$ s and $t_2 = 0.05$ s, respectively.[14] Table I shows the values of E_a obtained for regions R1 to R5 and their sum. The sum of the contributions of regions R1 to R5, $E_a = 40.73$ mW/m, is much larger than the contributions of $E_a = 2.20$ mW/m for region Ed and $E_a = -4.89$ mW/m for region Eu (not shown in the table).[14] Therefore, the main energy transfer from the fluid field to the acoustic field is caused by the interaction of the jet motion with the acoustic field, while the vortices shed by the collision of the jet with the edge in regions Ed and Eu make a minor contribution to the generation and absorption of acoustic energy.

In the upstream regions R1 and R2, E_a takes small negative values, although E_a takes positive values in the downstream regions R3, R4, and R5, especially in R4 and R5. Therefore, the acoustic energy is mainly generated in the downstream part of the jet close to the edge, while part of the acoustic energy seems to be lost in the upstream part, which is used to synchronize the jet with it.

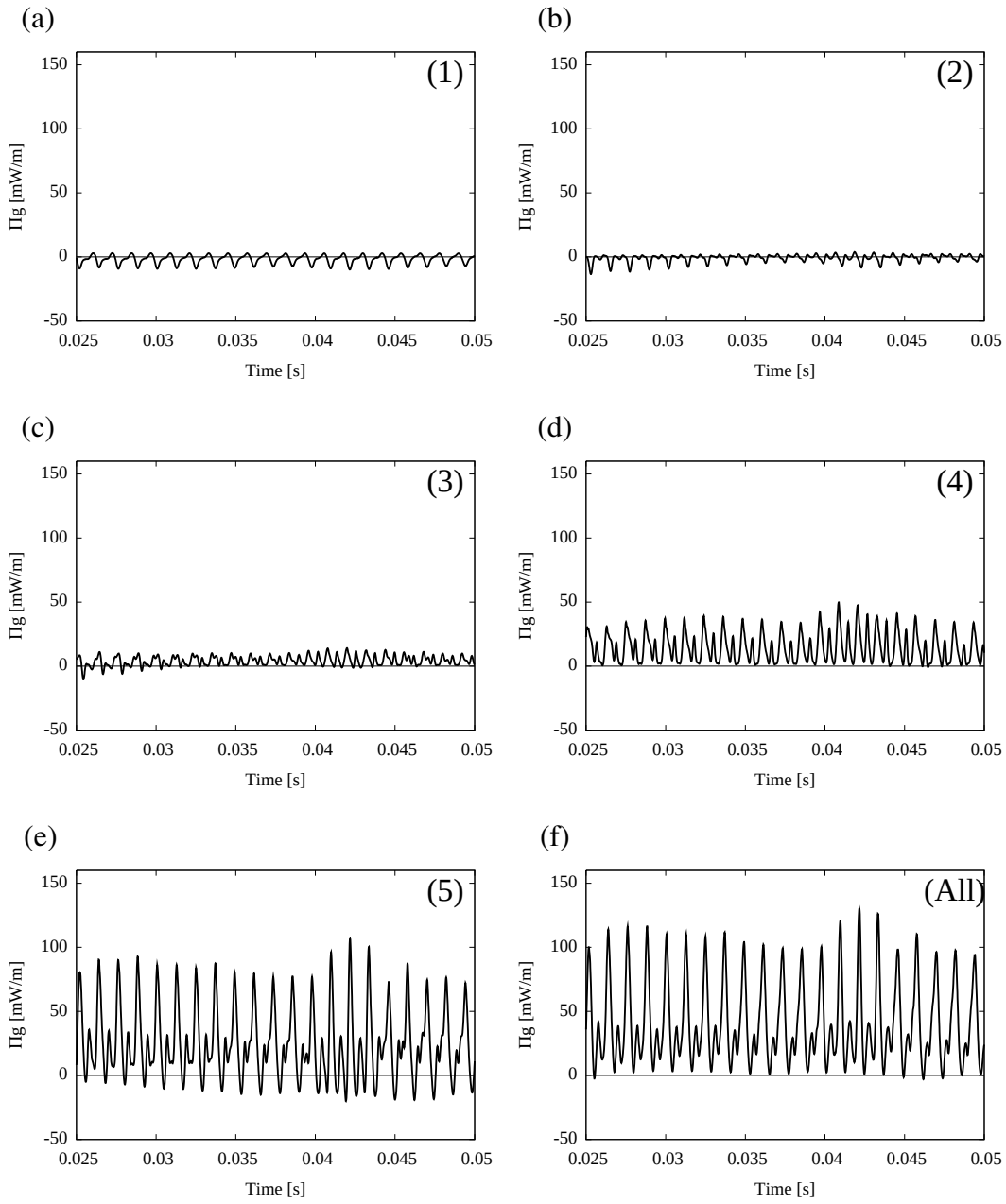

Fig. 4. Time evolution of Π_g region by region in the time interval $0.025 \leq t \leq 0.05$s. The labels from (1) to (5) in (a)-(e) indicate the integration regions from R1 to R5 in figure 3, respectively. The label (All) in (f) is the sum of Π_g for regions R1 to R5.

4.2 Comparison of the jet models with the numerical result of the 2D flue instrument model

Here we compare the jet models, i.e., the exponential and polynomial models, with the numerical result of the 2D flue instrument model in the previous paper.[14] For comparison, we take the semithickness of the jet as $b = d/2 = 0.5$mm, the jet velocity as $V = 12$ m/s, and the oscillation frequency as $f = 830$ Hz ($\omega = 2\pi f$), which gives the pitch of the instrument.

Table I. Acoustic energy generation for the 2D flue instrument model.

region	R1	R2	R3	R4	R5	total
E_a [mW/m]	-1.81	-0.85	4.17	14.46	24.76	40.73

Given the maximum acoustic pressure p_0 in the resonance pipe, the maximum acoustic particle velocity at the mouth opening of the flue instrument is estimated as $u_0 = p_0/c_0\rho_0 \times h/l$, where c_0 is the speed of sound and ρ_0 is the density of the air in equilibrium.[14,23] When the acoustic pressure is set at $p_0 = 100$ Pa, we obtain $u_0 \approx 0.49$ m/s for $\rho_0 \approx 1.2\text{kg/m}^3$ and $c_0 \approx 340$ m/s. For simplicity, we take $u_0 = 0.5$ m/s and u_w and μ are set as $V/2$ and ω/u_w, respectively.[1,15]

Fig.5 shows the velocity distributions of the exponential model and cubic polynomial model at $t = 2T/12$ ($T = 2\pi/\omega$), where the jets take similar positions to the jet in Fig.3 (a). For the exponential model in Fig.5 (a), the jet is extremely and unnaturally bent near the right end at $x = 5$mm, where the edge exists for the 2D flue instrument model, compared with that shown numerically in Fig. 3 (a). Furthermore, its amplitude takes unphysically large values such as $|\hat{y}| \approx 7$mm at $t = 0$ and $t = T/2$ (not shown in the figure). On the other hand, the profile of the jet for the cubic polynomial model in Fig.5 (b) is rather similar to that obtained numerically and its amplitude $|\hat{y}|$ does not exceed the reasonable value of 2.5mm at any time in the time period or at any point in the range $0 \le x \le 5$mm.

Furthermore, to estimate the net energy transfer from the fluid field to the acoustic field and vice versa, we calculate the time average of Π_g in each region for the individual models. Here, we take a time average over one period T,

$$E_a = \frac{1}{T}\int_0^T \Pi_g(t)\,\mathrm{d}t, \tag{34}$$

although we define the time average over a long time interval including a number of periods in Eq. (33). This is because Π_g numerically obtained for the 2D flue instrument model is not completely periodic with small fluctuations; thus, we need to take a long time interval to calculate the time average of Π_g. The time averages E_a in individual regions and in the whole region for all the models are shown in Table II. As expected from Eq. (30) and the discussion following it, E_a takes negative values in the upstream regions R1 and R2 and positive values in the downstream regions R3, R4, and R5 for all the models. This characteristic is the same as that for the 2D flue instrument model. However, the value of E_a in the whole region increases with the degree of the polynomial and it takes a very large value for the exponential model. As

Table II. Acoustic energy generation E_a [mW/m] for the polynomial and exponential models; P2: quadratic polynomial model, P3: cubic polynomial model, P4: quartic polynomial model, Exp: exponential model.

	region					
model	R1	R2	R3	R4	R5	total
P2	-3.07	-1.52	4.31	8.56	4.82	13.10
P3	-3.66	-3.81	4.94	17.92	17.90	33.29
P4	-3.83	-5.31	4.40	27.41	39.08	61.75
Exp	-3.87	-6.33	2.50	43.73	124.26	160.29

a result, the cubic polynomial model takes a reasonable value of E_a, i.e., $E_a \approx 33.29$mW/m, compared with that for the 2D flue instrumental model, $E_a \approx 40.73$ mW/m. Furthermore, it takes a value close to that for the 2D flue instrument model in every domain of integration. From the quantitative viewpoint, the cubic model is in good agreement with the 2D instrument model at least for the parameter values $b = d/2 = 0.5$mm, $V = 12$ m/s, $f = 830$ Hz, and $u_0 = 0.5$ m/s. Note that the jet profile and amplitude nonlinearly change with the jet velocity.[24] Thus, the cubic polynomial model may not be the best model throughout the physically important range of the jet velocity.

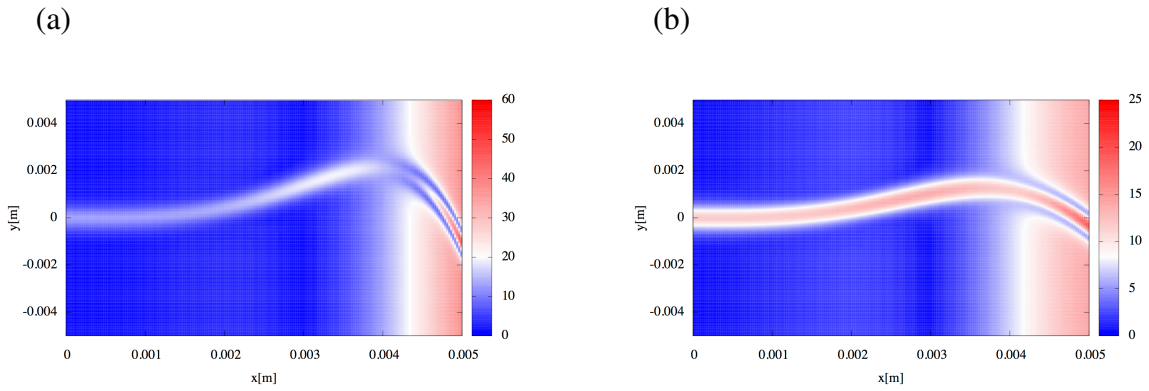

Fig. 5. (Color online) Spatial distributions of $|v|$ for the exponential model and cubic polynomial model at $t = 2T/12$. (a) Exponential model. (b) Cubic polynomial model.

4.3 Numerical estimation of Π_{gker} and Π_g with the jet models

In this subsection, we concentrate on the cubic polynomial model to investigate the properties of the integrand Π_{gker} and integral Π_g in the individual regions. Fig.6 shows the change in Π_{gker} in a half period for the cubic polynomial model at $V = 12$ m/s, $u_0 = 0.5$ m/s, and

$f = 830$ Hz. We observe qualitatively the same behavior of Π_{gker} as that numerically obtained for the 2D flue instrument.

The distribution of Π_{gker} is governed by the first term on the final line of Eq. (16). Thus, it takes negative and positive values along the upper and lower sides of the jet, respectively, if $u_y > 0$ as shown in (a)-(c), but it takes opposite values, positive at the upper side and negative at the lower side, if $u_y < 0$ as shown in (d) and (e). Note that since $u_y = 0$ at $t = 3T/12$ and $\Pi_{gker} = 0$, we omit this case in Fig.6.

As in the case of the 2D flue instrument model in Sect. 4.1, we divide the region of $0 \leq x < 5$mm into five regions from R1 to R5. To obtain Π_g as a function of time for each region and for the whole region ($0 \leq x < 5$mm), we integrate Π_{gker} with respect to y from $-\infty$ to ∞ and with respect to x over each region and the whole region. Fig.7 shows the time evolution of Π_g for regions R1 to R5 and for the whole region labeled All. The integrals Π_g oscillate with the same period T but with different oscillation amplitudes and different phases. The oscillation amplitude of Π_g becomes larger downstream. This is because, as shown in Eq. (24), the amplitude of Π_{gy} is governed by the terms of the monotonically increasing function $g(\mu x)$ and its derivatives. The increase in the amplitude downstream is also observed for the 2D flue instrument model as shown in Fig.4.

Since the jet forms a hydrodynamic wave, the phase difference between u_y and v_{yL} given by Eq. (9) changes with the observation point x. Fig.8 shows the spatial distribution of the Fourier component of v_y at the fundamental frequency $f = 830$ Hz. Fig. 8 (a) shows that the Fourier component of v_y takes large absolute values along the envelope of the jet oscillation, approximately obtained as $\pm\frac{u_0}{\omega}(g(\mu x) - 1)$ from Eq. (3). According to Eq. (10) and the discussion following it, v_{yL} leads u_y in phase by $\pi/4$ at the origin $(0, 0)$ and they coincide in phase at a small distance from the flue exit. As shown in Fig.8 (b), they coincide in phase at the point where $x \approx 1.2$mm and $y \approx 0$mm, and v_y lags behind u_y in phase with increasing x. This gives rise to the phase change of Π_g, which depends on the domain of integration. That is, the oscillations of Π_g are delayed in phase going downstream from R1 to R5. Actually, Π_g for R4 is almost out of phase by π compared with that for R1. As a result, in regions R1 and R2, where the jet oscillation is almost synchronized with the acoustic oscillation, Π_g takes negative values for most of the time period. On the other hand, in regions R3, R4, and R5, where it is almost out of phase with the acoustic oscillation, Π_g becomes positive in most of the time period. The total Π_g over the whole region slightly lags in phase behind that of R4 but leads that of R5, and it takes positive values almost all the time. The same tendency is also observed for the 2D flue instrument model, as shown in Fig.4, which indicates the

reliability of the jet model. However, the fluctuations of Π_g for the 2D instrument model are more complicated due to the irregularity of the fluid field and the acoustic field caused by the existence of the solid edge and resonance pipe.

Let us reconsider the time average E_a for the cubic polynomial model. Reflecting the properties of Π_g in the individual regions, E_a takes negative values in the upstream regions R1 and R2 and positive values in the downstream regions R3, R4, and R5 (see Table II). The value of E_a in each region is on the same order as that in the same region of the 2D flue instrument model. Although, Π_g for R5 has a larger oscillation amplitude than that for R4, E_a for R4 takes a slightly larger value than that for R5. This is because, from the discussion in the last paragraph of Sect. 3.3, Π_{gy} estimated by Eq. (30) takes positive values in almost all the time period near $x \approx 3.6$mm, where $\omega x/u_w = \pi$, in region R4, although the parts of the time period in which it takes positive values are shorter in R5. For the 2D flue instrument model, however, E_a takes a larger value in R5 than in R4 and the behavior of the jet for the 2D flue instrument model is considerably different from that of the jet model due to the existence of the edge and the resonance pipe.

Since $|E_a|$ is larger in the downstream part than in the upstream part, E_a for the whole region takes a positive value, which means net acoustic energy generation from the oscillating jet. Therefore, the main acoustic source is located in the downstream part, although the absorption of acoustic energy occurs in the upstream part, where it is considered that part of the acoustic energy is consumed in forcing the jet to be synchronized with the acoustic oscillation. As a result, the estimation of Howe's formula with the cubic jet model is in good agreement with the numerical result for the 2D flue instrument model, though the jet model is very different in geometry from the 2D flue instrument model, for example, the nonexistence of the edge and resonance pipe and the uniformity of the acoustic particle velocity.

Finally, we consider the properties of $\bar{\Pi}_{gy}$ defined by Eq. (25) as a function of x, comparing the cubic polynomial model with the other models. Fig.9 shows the dependence of $\bar{\Pi}_{gy}$ on the jet model. With increasing degree of the polynomial, the oscillation amplitude of $\bar{\Pi}_{gy}$ grows, especially in the downstream part, where the jet is largely curved. For the exponential model, $\bar{\Pi}_{gy}$ takes unphysically large values for $x > 3$mm. Nevertheless, all the models qualitatively show the same property: they take negative values in the upstream part but positive values in the downstream part (also see Table II). This indicates that the choice of the jet model, i.e., the function $g(\mu x)$, is important so that the calculation of Howe's energy corollary is in quantitatively good agreement with the numerical result for the flue instrument model[14] as well as the experimental result.[13]

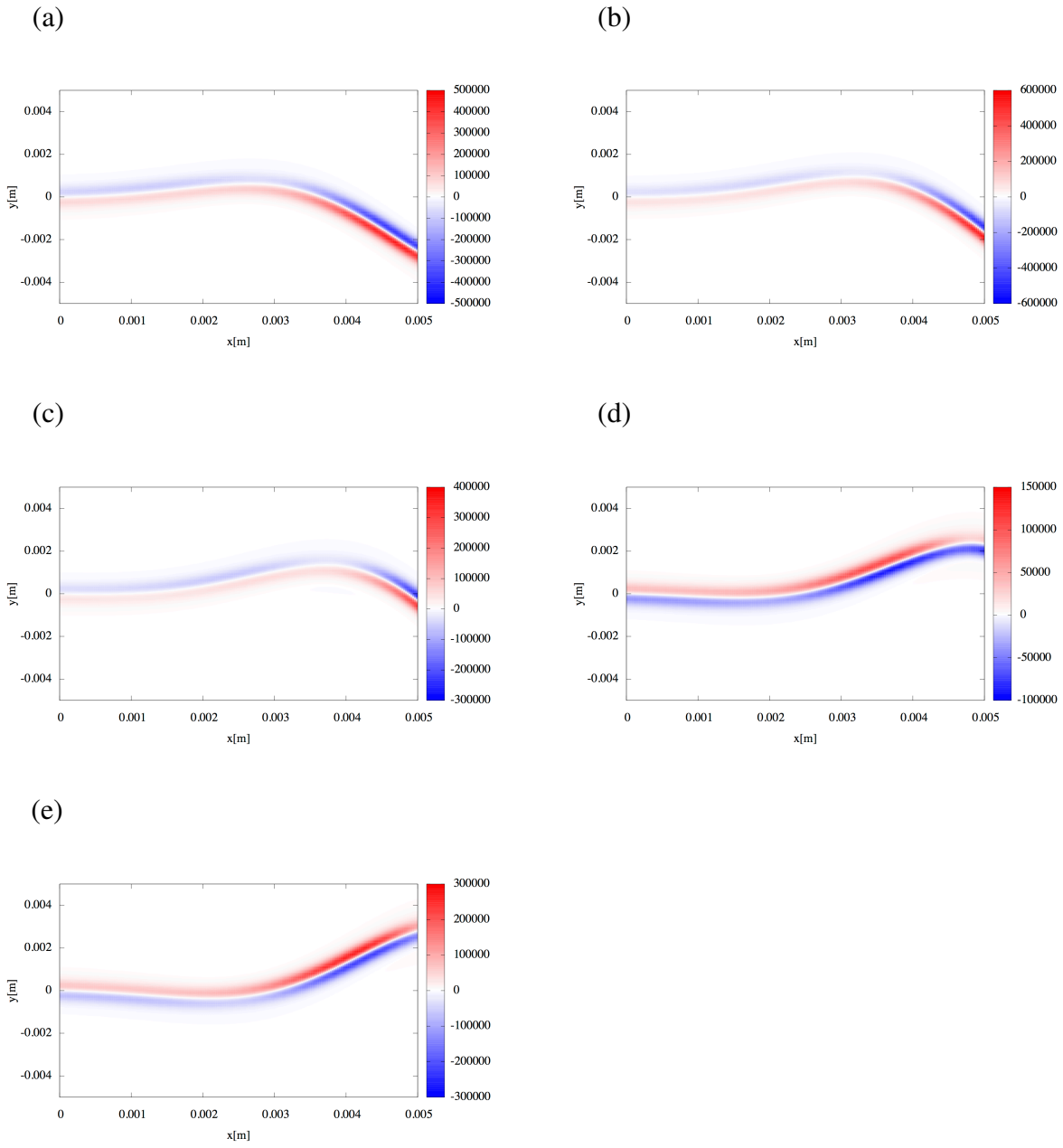

Fig. 6. (Color online) Time evolution of Π_{gker} for the cubic polynomial model in the first half period ($0 \leq t < T/2$). Π_{gker} at $t = T/3$ is omitted because $u_y = 0$ and $\Pi_{gker} = 0$. (a) $t = 0$, $u_y > 0$. (b) $t = T/12$, $u_y > 0$. (c) $t = 2T/12$, $u_y > 0$. (d) $t = 4T/12$, $u_y < 0$. (e) $t = 5T/12$, $u_y < 0$.

5. Summary and Discussion

In this paper, using Howe's energy corollary, we have studied the acoustic energy generation and absorption caused by the interaction between a jet and an acoustic field. To do this, we have introduced polynomial and exponential jet models and have calculated Howe's integrand Π_{gker} and integral Π_g for them, comparing the results with the numerical results for

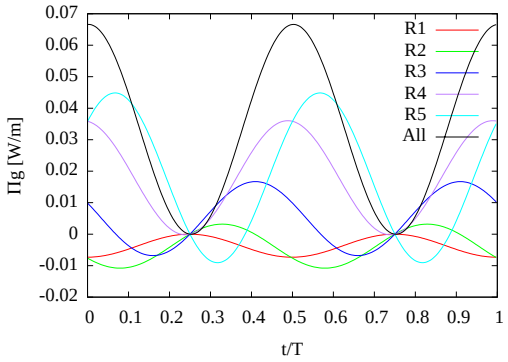

Fig. 7. (Color online) Time evolution of Π_g for the cubic polynomial model in regions R1 to R5 and in the whole region labeled All.

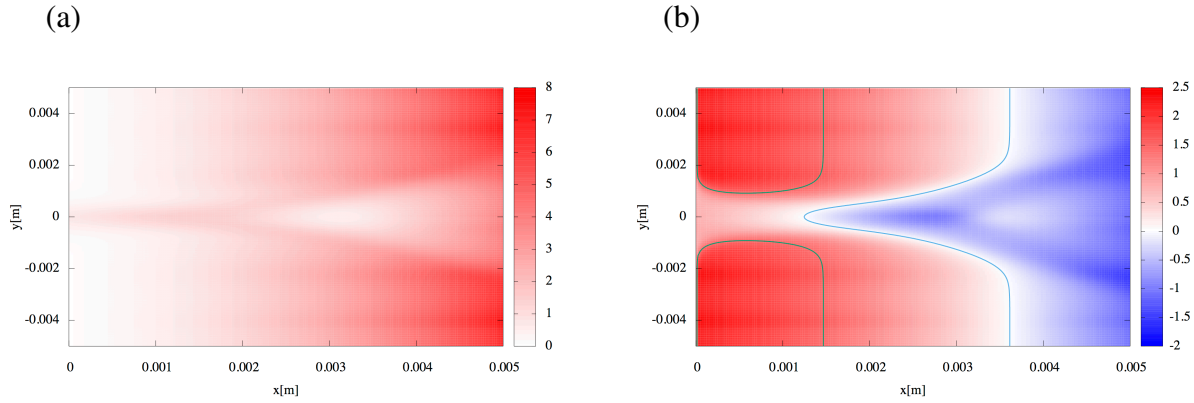

Fig. 8. (Color online) Fourier component of v_y at $f = 830$ Hz. (a) Distribution of the absolute value. (b) Distribution of the phase shift relative to the acoustic oscillation. Contours representing the values of 0 and $\pi/2$ are drawn.

the 2D flue instrument model studied in our previous paper.[14)]

It was found that the behavior of the cubic polynomial model is very similar to that of the jet observed for the 2D flue instrument model in the present situation. The oscillations of the other polynomial models and of the exponential model are qualitatively similar to that of the 2D flue instrument model but do not show quantitative agreement, such as an unphysically large amplitude for the exponential model. On the other hand, the amplitude for the cubic polynomial model is on the same order as that for the 2D flue instrument model.

Furthermore, the spatial distributions of Howe's integrand Π_{gker} for the jet models are in good agreement with that for the 2D flue instrument model. Namely, it takes negative and positive values along the upper and lower sides of the jet, respectively, when $u_y > 0$, but it takes opposite values when $u_y < 0$. Thus, Π_{gker} appears to be an odd function of $y - \hat{y}(x,t)$,

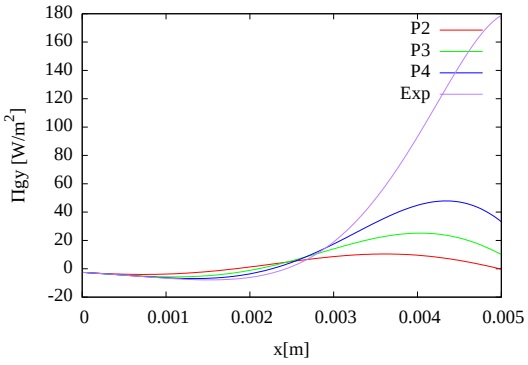

Fig. 9. (Color online) $\bar{\Pi}_{gy}$ for the polynomial and exponential models; P2: quadratic polynomial model, P3: cubic polynomial model, P4: quartic polynomial model, Exp: exponential model.

where $\hat{y}(x,t)$ is the centerline of the wavy jet. However, it involves even function components, which are caused by the skew symmetry of the bending jet. Actually, terms including the even components of the shearing velocity $\frac{\partial v_y}{\partial x}$ appear in Π_{gker} and contribute to the acoustic energy generation and absorption, while the odd function component does not make any contribution because its integral with respect to y takes a value of zero.

Since the values of Π_{gy}, i.e., the integral of Π_{gker} with respect to y, change with the position x, the amount of generation or absorption of acoustic energy changes along the jet. The time average of Π_{gy}, i.e., $\bar{\Pi}_{gy}$, indicates that acoustic energy absorption $\bar{\Pi}_{gy} < 0$ occurs in upstream regions near the flue exit, where the jet motion is nearly synchronized with the acoustic field, while acoustic energy generation $\bar{\Pi}_{gy} > 0$ occurs in downstream regions, where the jet oscillation is nearly out of phase with the acoustic oscillation. Therefore, the amount of acoustic energy generation or absorption is controlled by the relative phase between the jet oscillation and the acoustic oscillation as pointed out by Yoshikawa *et al.*[13] Concerning the absorption in the upstream region, it is considered that part of the acoustic energy is consumed in forcing the jet to be synchronized with the acoustic oscillation.

To compare the theoretical estimation of Howe's integral by the cubic polynomial model with the numerical result for the 2D flue instrument model, we have integrated Π_{gker} region by region, i.e., regions R1 to R5, and have taken their time averages E_a. The theoretical estimation of the integral Π_g in each region is qualitatively and quantitatively in good agreement with that for the 2D flue instrument model. The amount of acoustic energy absorption in the upstream region is much smaller than that of acoustic energy generation in the downstream region; thus, net acoustic energy generation is observed. The time average E_a obtained theoretically takes a value in each region close to that obtained by the numerical simulation by the

2D flue instrument model.[14] Furthermore, the experimental result reported by Yoshikawa *et al.*[13] shows a similar tendency qualitatively and quantitatively. Therefore, the jet models introduced in this paper, especially the cubic polynomial model, well explain the mechanism of acoustic energy generation and absorption caused by the interaction between the oscillating jet and the acoustic field based on Howe's energy corollary.

The jet models introduced in this paper can be applied to other objects. For example, to study the generation of acoustic waves directly, we require Lighthill's acoustic analogy[4] and the theories following it.[3,5] In this context, the generation of acoustic waves from an oscillating jet, which occurs for the cases of edge tone and flue instruments, is still an open problem.[1–3] By using our jet models, we can investigate in detail the properties of the principal term of Lighthill's source under the incompressible fluid approximation, for example, the spatial distribution of the source term and its time evolution. We expect that the comparison of the theoretical estimation based on the jet models with numerical simulations for edge tone models and flue instrument models will allow us to consider the meaning of Lighthill's source and to clarify the properties of sound waves radiating from a source and propagating to a far field. We will leave these studies to a future work.

Appendix

Under the assumption that a planar jet is not affected by the acoustic particle velocity or pressure gradient, Bickley examined the velocity profile of a stationary jet of an incompressible fluid, which changes in the horizontal direction, i.e., along the x-axis, due to the air viscosity ν.[16] It is known that the velocity profile predicted by Bickley's theory is in good agreement with experimental results.[1,20] The resultant profile of v_x is given by[1,16]

$$v_x(x,y) = \alpha\left(\frac{J^2}{\nu x}\right)^{1/3} \mathrm{sech}^2(y/b), \tag{A·1}$$

where b and J are defined by

$$b = \beta\left(\frac{\nu^2}{J}\right)^{1/3} x^{2/3}, \tag{A·2}$$

$$J = \int_{-\infty}^{\infty} v_x(x,y)^2 \mathrm{d}y. \tag{A·3}$$

Since $\rho_0 J$ is the momentum passing per unit time through the vertical plane at $x = \text{const.}$, J should be constant due to the conservation of momentum. From the equality

$$\int_{-\infty}^{\infty} \mathrm{sech}^4(z)\mathrm{d}z = \left[\tanh z - \frac{1}{3}\tanh^3 Z\right]_{-\infty}^{\infty} = 4/3, \tag{A·4}$$

Eq. (A·3) is reduced to $J = \frac{4}{3}\alpha^2\beta J$ and $\alpha^2\beta = 3/4$. Bickley took $\alpha = \frac{1}{2}(\frac{16}{9})^{-1/6} \approx 0.4543$ and $\beta = 3(\frac{16}{9})^{1/3} \approx 3.634$.

Suppose that the exit of the flue is at $x = x_0$ and the jet velocity at the center of the exit is $v_x(x_0, 0) = V$. Then, we obtain

$$V = \alpha\left(\frac{J^2}{\nu x_0}\right)^{1/3}. \tag{A·5}$$

Since the semithickness of the jet is $b = b_0$ at $x = x_0$, Eq. (A·3) is rewritten as

$$J = \int_{-\infty}^{\infty} V^2 \mathrm{sech}^4(y/b_0)\mathrm{d}y = \frac{4}{3}V^2 b_0. \tag{A·6}$$

Therefore, x_0 is given by a function of V and b_0,

$$x_0 = \alpha^3 \frac{16 V b_0^2}{9\nu}, \tag{A·7}$$

and $v_x(x, 0)$ and $b(x)$ are obtained as

$$v_x(x, 0) = V(x_0/x)^{1/3}, \tag{A·8}$$

$$b(x) = b_0(x/x_0)^{2/3}. \tag{A·9}$$

For $V = 12$ m/s, $b_0 = 5 \times 10^{-4}$ m, and $\nu = 1.5 \times 10^{-5}$ m^{2}s^{-1}, the flue exit is located at $x_0 = 1/30 \approx 0.03333$ m. Then at the point 5mm downstream from the flue exit, i.e., $x = x_0 + 0.005$ m and $y = 0$ m, v_x and b are given by $v_x \approx 0.9545V$ and $b \approx 1.098b_0$, respectively.

It is not easy to precisely estimate the reduction rate of the velocity v_x along the centerline of the oscillating jet for the 2D flue instrumental model because it is fluctuating due to the oscillation. As a rough estimation, the reduction rate at the point $x = 4$ mm downstream from the flue exit, i.e., 1 mm upstream from the edge, is in the range of 0.82 – 0.95, which is slightly smaller than the theoretical estimation of $v_x/V \approx 0.9629$. Anyhow, it is expected that the jet velocity will not be significantly reduced between the flue exit and the edge.

References

1) N. H. Fletcher and T. D. Rossing, *The Physics of Musical Instruments* (Springer-Verlag, New York, 1998) 2nd ed.

2) B. Fabre, J. Gilbert, A. Hirschberg, and X. Pelorson, Annu. Rev. Fluid Mech. **44**, 1 (2012).

3) M. S. Howe, *Acoustics of Fluid-Structure Interactions* (Cambridge Univ. Press, Cambridge, 1998).

4) M. J. Lighthill, Proc. R. Soc. London, Ser. A **211**, 564 (1952).

5) M. E. Goldstein, *Aeroacoustics* (McGraw-Hill, New York, 1976).

6) M. E. Goldstein, J. Fluid Mech. **488**, 315 (2003).

7) M. E. Goldstein, J. Fluid Mech. **526**, 337 (2005).

8) A. Powell, J. Acoust. Soc. Am. **36**, 177 (1964).

9) M. S. Howe, J. Fluid Mech. **71**, 625 (1975).

10) M. S. Howe, IMA J. Appl. Math. **32**, 187 (1984)

11) A. Bamberger, Forum Acusticum Budapest 2005, 4th Eur. Cong. Acoustics, 2005, p.665.

12) S. L. Finnegan, C. Meskell, and S. Ziada, J. Pressure Vessel Technol. **132**, 041306 (2010).

13) S. Yoshikawa, H. Tashiro, and Y. Sakamoto, J. Sound Vib. **331**, 2558 (2012).

14) T. Kobayashi, T. Akamura, Y. Nagao, T. Iwasaki, K. Nakano, K. Takahashi, and M. Aoyagi, Fluid Dyn. Res. **46**, 061411 (2014).

15) M. Miyamoto, Y. Ito, T. Iwasaki, T. Akamura, K. Takahashi, T. Takami, T. Kobayashi, A. Nishida, and M. Aoyagi, Acta Acust. United. Ac. **99**, 154 (2013).

16) W. G. Bickley, Philos. Mag. **23**, 727 (1937).

17) N. H. Fletcher and S. Thwaites, Acustica **42**, 323 (1979).

18) S. A. Elder, J. Acoust. Soc. Am. **64**, 877 (1978).

19) S. A. Elder, J. Acoust. Soc. Am. **67**, 774 (1980).

20) A. W. Nolle, J. Acoust. Soc. Am. **103**, 3690 (1998).

21) B. Fabre and A. Hirschberg, Acta Acust. United. Ac. **86**, 599 (2000).

22) C. Wagner, T. Hüttl, and P. Sagaut, eds. *Large-Eddy Simulation for Acoustics* (Cambridge Univ. Press, New York, 2007).

23) M. P. Verge, B. Fabre, and A. Hirschberg, J. Acoust. Soc. Am. **101**, 2914 (1997).

24) B. Fabre, A. Hirschberg, and A. P. J. Wijnands, Acta Acust. United. Ac. **82**, 863 (1996).